Office of Naval Research
DEPARTMENT OF THE NAVY
Contract N6onr-24420 (NR 062-059)

ON THE MECHANISM OF CAVITATION DAMAGE

M. S. Plesset and A. T. Ellis

Hydrodynamics Laboratory
CALIFORNIA INSTITUTE OF TECHNOLOGY
Pasadena, California

Report No. 21-15

JUNE, 1954

ABSTRACT

A new method for producing cavitation damage in the laboratory is described in which the test specimen has no mechanical accelerations applied to it in contrast with the conventional magnetostriction device. Alternating pressures are generated in the water over the specimen by exciting a resonance in the "water cavity". By this means the effects of cavitation have been studied for a variety of materials. Photomicrographs have been taken of several ordinary (polycrystalline) specimens and also of zinc monocrystals. The zinc monocrystal has been exposed to cavitation damage on its basal plane and also on its twinning plane. X-ray analyses have been made of polycrystalline specimens with various exposures to cavitation. The results show that plastic deformation occurs in the specimens so that the damage results from cold-work of the material which leads to fatigue and failure.

A variety of materials have been exposed to intense cavitation for extended periods to get a relative determination of their resistance to cavitation damage. It is found that, roughly speaking, hard materials of high tensile strengths are the most resistant to damage. While this survey is far from complete it has been found that titanium 150-A and tungsten are the most resistant to damage of the materials tested.

INTRODUCTION

Numerous studies have been made of the cavitation process and the mechanism of cavitation damage. No attempt will be made here to give a bibliography on this subject; reference may be made, however, to the monograph by Nowotny (1) and to an investigation of damage with a magnetostriction oscillator by Kornfeld and Suvorov (2). In laboratory studies of cavitation damage it is often desirable to accelerate the damage rate. It has long been recognized that the cavitation produced by pressure variations at relatively

high frequencies will produce damage more rapidly than the cavitation under ordinary flow conditions. The procedure which has been universally used consists in high frequency acceleration of the test specimen relative to the liquid medium. These accelerations are obtained by application of the magnetostrictive effect in a nickel rod to the end of which the test specimen is attached. The liquid partakes of this accelerating motion and heavy cavitation is produced (cf. Ref. 1 and 2). In such experiments the quantities measured are the displacement of the test surface and its frequency. Weight loss of the specimen is also determined as a function of exposure time to the cavitation field.

A new method for generating cavitation damage has been developed and studied by one of the authors (3) and appears to have some important advantages for this type of investigation. While this method is described in detail in Ref. (3), it is necessary to give a brief description of it here so that the results of the present study may be more easily interpreted.

PRESSURE VARIATIONS PRODUCED IN A RESONANT CAVITY

The apparatus used consists of a cylindrical beaker containing water with a barium titanate ring just below the surface (Fig. 1). If an alternating electric field is applied across the conducting coatings on the inner and outer surfaces of the ring, the volume of the ring oscillates with the applied electric field. At the proper frequency of the electric field, a standing wave pattern is set up in such a way that a large pressure amplitude is produced at the center of the bottom plate. The pressure variation is sufficient to produce cavitation over the specimen with a sinusoidal voltage of amplitude between 100 to 200 volts. For some of the experiments, the oscillation frequency was 18,000 cycles; for the remainder of the studies, with a beaker of different dimensions, the oscillation frequency was 24,000 cycles. Figure 2 shows the well-defined cavitation cloud over the surface of the specimen. Figure 3 shows the complete apparatus with the audio oscillator, the power amplifier, and the beaker.

The acoustic theory for the pressure field in a cylindrical cavity is easily developed. The fluid velocity $\bar{v}$ and the time varying part of the pressure p are related to the velocity potential φ by $\bar{v} = -\nabla\varphi$ and $p = \rho_w \partial\varphi/\partial t$, where ρ_w is the density of water. Viscous and streaming effects are neglected. One seeks a characteristic solution of the wave equation

$$\Delta\varphi - \frac{1}{c^2}\frac{\partial^2\varphi}{\partial t^2} = 0 \qquad (1)$$

of the form $\varphi = R(r)\,Q(z)\,e^{i\omega t}$ where c is the sound velocity in water, $\omega/2\pi$ is the exciting frequency, r is the radial distance from the axis of cylindrical symmetry, and z is the distance measured along this axis (cf. Fig. 1). The origin of z is at the water surface and the positive direction of z is upward. The boundary conditions may be described as follows. The massive steel plate at the bottom of the container is assumed to move as a free rigid mass. Under this assumption, Newton's second law of motion gives a condition on the velocity potential at the interface of the liquid and the steel plate:

$$\rho_w \frac{\partial\varphi}{\partial t} - \frac{d}{dt}\left(\frac{\partial\varphi}{\partial z}\right)(\rho_s d) = 0, \qquad \text{at} \quad z = -\ell\,;$$

or

$$\varphi - \frac{\partial\varphi}{\partial z}\left(\frac{\rho_s d}{\rho_w}\right) = 0, \qquad \text{at} \quad z = -\ell\,; \qquad (2)$$

where ρ_s is the density of the steel plate and d is its thickness. The boundary condition at the beaker wall is determined under the assumption that this wall is under simple hoop tension. The force per unit length of the cylindrical wall is $Ebda/a$ where E is the Young's modulus of the glass (pyrex), b is its thickness, and a is its unstrained radius. Then the force equation at the wall, $r = a$, leads to the boundary condition

$$\varphi - \left(\frac{E}{a^2\omega^2} - \rho_g\right)\frac{b}{\rho_w}\frac{\partial\varphi}{\partial r} = 0, \qquad \text{at} \quad r = a\,; \qquad (3)$$

where ρ_g is the density of the glass. There is, finally, the boundary condition at the free surface of the water:

$$\varphi = 0, \qquad \text{at} \quad z = 0\,. \qquad (4)$$

The characteristic solutions which satisfy these boundary conditions are

$$\varphi_{mn} = A_{mn} \sin\beta_m z \; J_o\left[\left(\frac{\omega_{mn}^2}{c^2} - \beta_m\right)^{1/2} r\right] \qquad (5)$$

where J_o is the Bessel function of zero order and β_m is a solution of the equation

$$\frac{\tan \beta \ell}{\beta} = - \frac{\rho_s d}{\rho_w} .$$

The angular frequency ω_{mn} is given by

$$\omega_{mn} = c \left[\left(\frac{\alpha_{mn}}{a} \right)^2 + \beta_m^2 \right]^{1/2} ;$$

where the constant α_{mn} is determined from the solution of the equation

$$\frac{J_o(\alpha)}{\alpha J_1(\alpha)} = \frac{b}{a} \left\{ \frac{\rho_g}{\rho_w} - \frac{E}{\rho_w c^2 \left[\alpha^2 + a^2 \beta_m^2 \right]} \right\} .$$

A series of characteristic frequencies have been computed and have been compared with measured resonant frequencies for the "water cavity". Agreement between theoretical and observed values is very good. The pressure amplitude has been measured as a function of r and z. These variations also agree well with those determined by Eq. (5). Of immediate practical importance is that the most easily excited mode has the largest pressure amplitude at the center of the bottom plate. Thus, the cavitation cloud is readily confined to the small region over the specimen. Figure 4 shows the cavitation bubble cloud at two different points of the pressure cycle. The upper picture shows the bubble cloud near the pressure maximum and the lower picture shows the bubble cloud near the pressure minimum. Figure 5 gives somewhat greater detail in the bubble cloud near the maximum (the lower half of the picture is a reflection of bubble cloud in the stainless steel plate).

In the opinion of the authors, the method used here for producing cavitation damage in the laboratory has several important advantages over the magnetostriction oscillator method. The use of the barium titanate electric transducer to generate standing pressure waves in the water "cavity" results in an apparatus which is very simple electrically and which, at the same time, is appreciably less expensive than the magnetostriction oscillator. The present device is stable in operation and requires a minimum of maintenance and attention. A wide range of frequencies is readily available. Of perhaps

greater significance is the fact that one has here an efficient way of producing the oscillating cavitation field. As a consequence, there is negligible heating of the water or the test specimen even in very long exposures at high powers. Under heavy cavitation conditions, the water temperature has been observed to rise less than $3^{\circ}C$ in one hour. It should also be remarked that there is negligible streaming of the water in the container and there is no pumping action on the water. An additional consideration which led the authors to the adoption of this resonant "cavity" procedure was the fact that the test specimen is stationary throughout its exposure to cavitation. There are no mechanical acceleration stresses applied to the specimen as there are when it is attached to a magnetostriction rod. As a specimen receives cavitation damage, small regions of reduced strength are produced and these small regions might be torn out of the specimen under mechanical acceleration. From the point of view of an analytic consideration of the cavitation bubble behavior, it would also seem advantageous to have a stationary boundary and no gross water velocity or acceleration.

PHOTOMICROGRAPHIC OBSERVATIONS OF CAVITATION DAMAGE

A series of experiments were made to observe the optical changes in the surface of a specimen under cavitation damage. Figure 6 shows the surface of a nickel specimen after a 5 minute exposure to the cavitation cloud. It is of interest to note the uneveness of the damaged surface. This appearance of microscopic "hills and valleys" is characteristic of the behavior of very soft materials. Figure 7 shows a stainless steel specimen which is of somewhat greater interest, metallurgically, since slip lines are clearly in evidence. These results may be compared with the photomicrographs of a harder material, an example of which is titanium 130-A (Fig. 8). No optical alteration in the surface of this material is evident even after prolonged exposure to the cavitation cloud.

This series of photomicrographs is typical of results with other materials. The very soft materials quickly show a microscopic hill and valley effect and not much can be deduced regarding crystallographic changes. In materials of intermediate hardness, this hill and valley effect is not so evident and some evidence of crystallographic changes may be observed. In the very hard materials no change is evident. In these studies, the cavitation damage was kept sufficiently light so that no significant weight loss in the specimens was

obtained. Optical observations and photomicrography appear to be of limited value for a polycrystalline material which is the usual state of a specimen.

A series of experiments were undertaken to secure a rough measure of resistance to cavitation damage in a series of polycrystalline substances. This series has definite engineering interest. To get significant damage quickly, the specimens were made with a small tip protruding above the level of the bottom flat plate. By this means the cavitation cloud was concentrated over the end of the tip and did not appear elsewhere. The area concentration so obtained gave an intensity increase by a factor of 25 over the conditions shown in Figs. 6, 7, and 8. With this configuration, the cavitation damage effectively drilled nearly cylindrical cavities in the specimens. The depth of these cylindrical holes for given exposure time is a measure of the resistance to damage. Measurements of this kind are summarized in Table I. A photograph of a stellite specimen exposed to this concentrated cloud is shown in Fig. 9, and a corresponding photograph of a titanium 150-A specimen is shown in Fig. 10.

Photomicrography can be a powerful tool in revealing alterations in crystal structure if the specimen is a single crystal. A zinc monocrystal was made available to the authors through the kindness of Dr. Thad Vreeland, Jr., of the Engineering Division, California Institute of Technology. A basal plane (0001 plane) was obtained for exposure to cavitation by cleavage in liquid nitrogen. When this surface is stressed by the cavitation field, the hexagonal structure of the exposed plane becomes evident. Figure 11 shows this effect when the surface is exposed to a cloud of extent small compared with the exposed area. The nearly point application of the cavitation stress brings out the hexagonal structure very readily. Figure 12 shows a basal plane in a zinc crystal before exposure to cavitation. Figures 13, 14, and 15 show this same specimen after exposure to a broad cloud of cavitation covering the specimen. Similar observations have been made on a zinc crystal cut parallel to a twinning plane and the results are shown in Figs. 16, 17, and 18. The geometry of the zinc crystal is sketched in Fig. 19.

While some of the previous photomicrographs gave evidence that cavitation damage is initiated through plastic deformation of the exposed specimen, very striking and detailed additional evidence of this mechanism are obtained from these studies on the monocrystal. In particular, severe plastic deformation of the zinc monocrystal is found in the form of twinning in the specimens

exposed on a slip plane and in the form of slip in the specimens exposed on a twinning plane.

X-RAY OBSERVATIONS OF CAVITATION DAMAGE

Changes in structure can be observed readily in a polycrystalline specimen by the use of X-rays. For this reason, a series of observations were made on ordinary specimens exposed to cavitation damage. Figure 20 shows X-ray diffraction patterns from a nickel specimen before exposure to cavitation, after 2 seconds exposure to a broad cavitation cloud, and after 10 seconds exposure. The blurring of the patterns, which is quite marked after only 2 seconds exposure, shows that plastic deformation of the nickel microcrystals starts almost immediately upon exposure to cavitation. Figure 21 shows entirely similar results in brass. These specimens showed no significant optical change or weight loss; yet the alteration in structure is very evident from the X-ray observations.

To determine the depth of the region of plastic deformation, thin layers were removed from the surface until the X-ray pattern returned approximately to its original configuration. Layers were "peeled off" uniformly by the process of electrolytic polishing. These results are illustrated in Figs. 22 and 23 for nickel, and in Fig. 24 for brass. A similar study was made of a pure titanium specimen and is illustrated in Fig. 25. Here the X-ray diffraction spots are replaced by circular lines since the specimen was rotated while being exposed to the X-ray beam. The broadening of the circular lines shows again the plastic deformation which takes place on exposure to cavitation. To determine the depth of penetration of the region of plastic deformation in titanium, layers were removed in steps by etching until the lines returned approximately to their original sharpness.

SUMMARY AND CONCLUSION

The apparatus for this study of cavitation damage, in the authors' opinion, is an inexpensive and efficient device for cavitation research or testing. Cavitation tests are extremely simple and relative resistance to cavitation damage such as is given in Table I is very easily obtained.

Ordinary polycrystalline specimens and pure monocrystals have been exposed to cavitation damage. Photomicrographic examination and X-ray

diffraction patterns both show that plastic deformation occurs. This plastic deformation appears to set in almost immediately in soft substances such as nickel, brass, or pure titanium. Since these are substances with ultimate tensile strengths of the order of 50,000 psi, it is indicated that cavitation stresses may be at least of this magnitude. On the other hand, the very slow onset of damage in a material such as tungsten or titanium 150-A with ultimate tensile strengths of the order of 130,000 psi or greater might be taken as an indication that cavitation stresses lie below this magnitude.

It should be emphasized that cavitation damage represents the interaction of a complex of properties of the solid so that consideration of ultimate tensile strengths alone, or of hardness alone, or any other single property would be misleading. The general mechanism of the damage does appear to be reasonably clear. A polycrystalline or monocrystalline specimen exposed to cavitation undergoes eventual or almost immediate plastic deformation depending on its hardness and yield properties. This plastic deformation is a cold-work of the material which leads to fatigue and failure of portions of the specimen.

ACKNOWLEDGMENTS

This study was supported by the U. S. Navy Office of Naval Research, Mechanics Branch. The authors wish to express their appreciation to Mr. J. E. Neimark for valuable assistance with the observations on zinc monocrystals. The authors are also greatly indebted to Professors Pol Duwez and David Wood of the Engineering Division of the California Institute of Technology not only for making facilities available to them but also for their helpful interest and comments throughout the study.

REFERENCES

1. H. Nowotny, Werkstoffzerstörung durch Kavitation (Edwards, 1946).

2. M. Kornfeld and L. Suvorov, On the Destructive Action of Cavitation, Journal of Applied Physics 15, 495 (1944).

3. A. T. Ellis, Production of Accelerated Cavitation Damage by an Acoustic Field in a Cylindrical Cavity, Hydrodynamics Laboratory Report No. 21-14, California Institute of Technology.

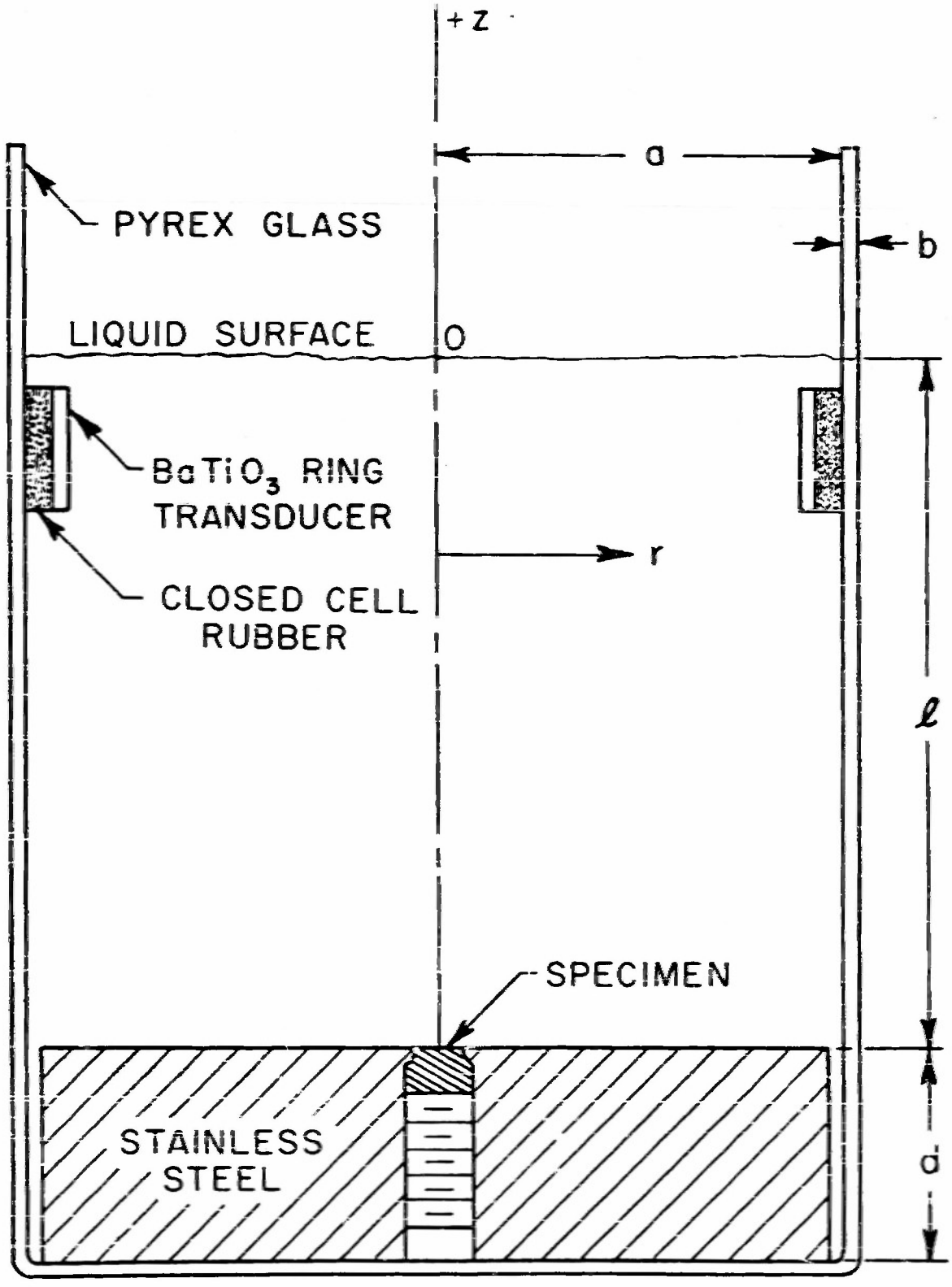

Fig. 1 - Diagram of cylindrical beaker and coordinate system.

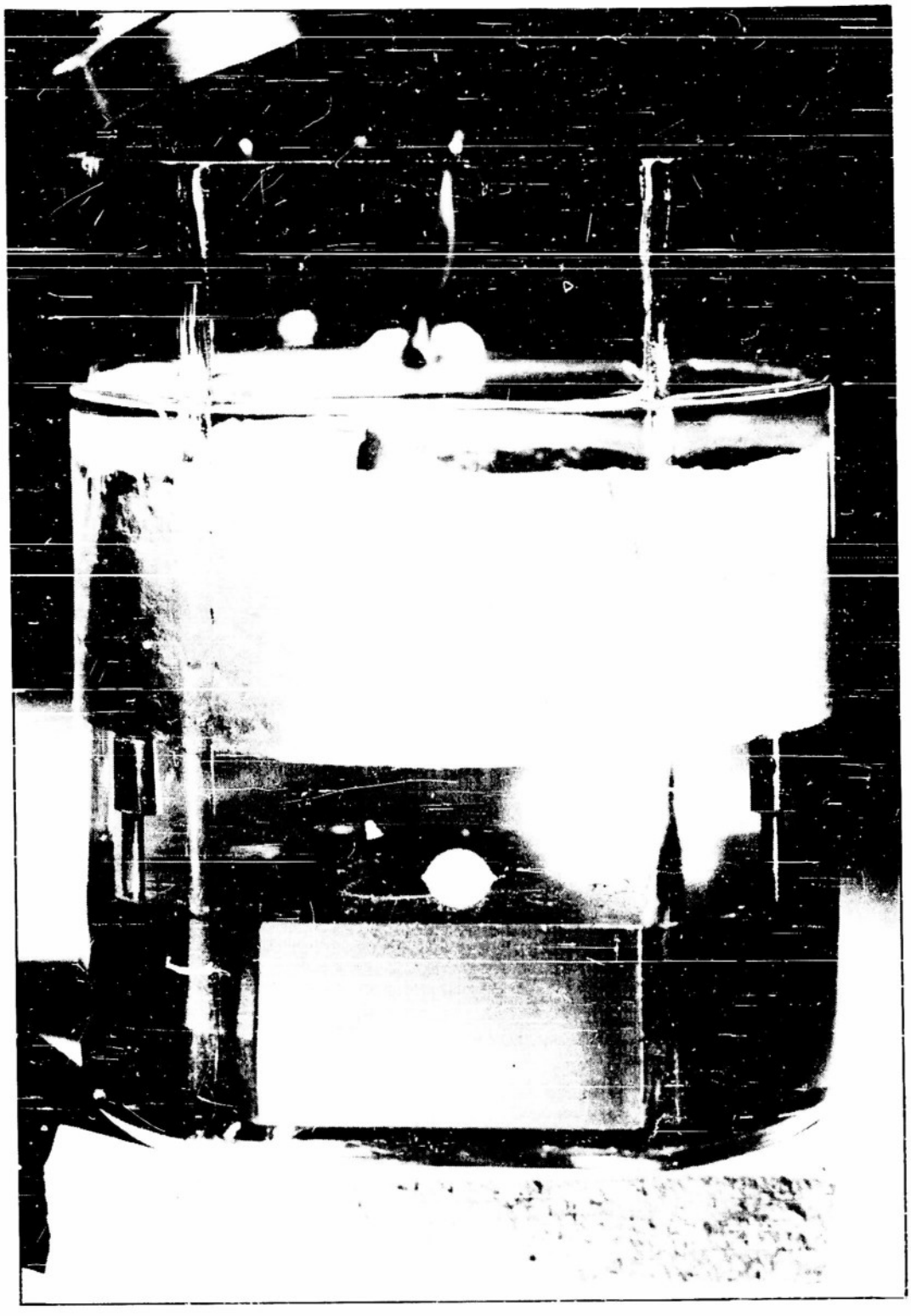

Fig. 2 - Beaker in operation showing cavitation cloud.

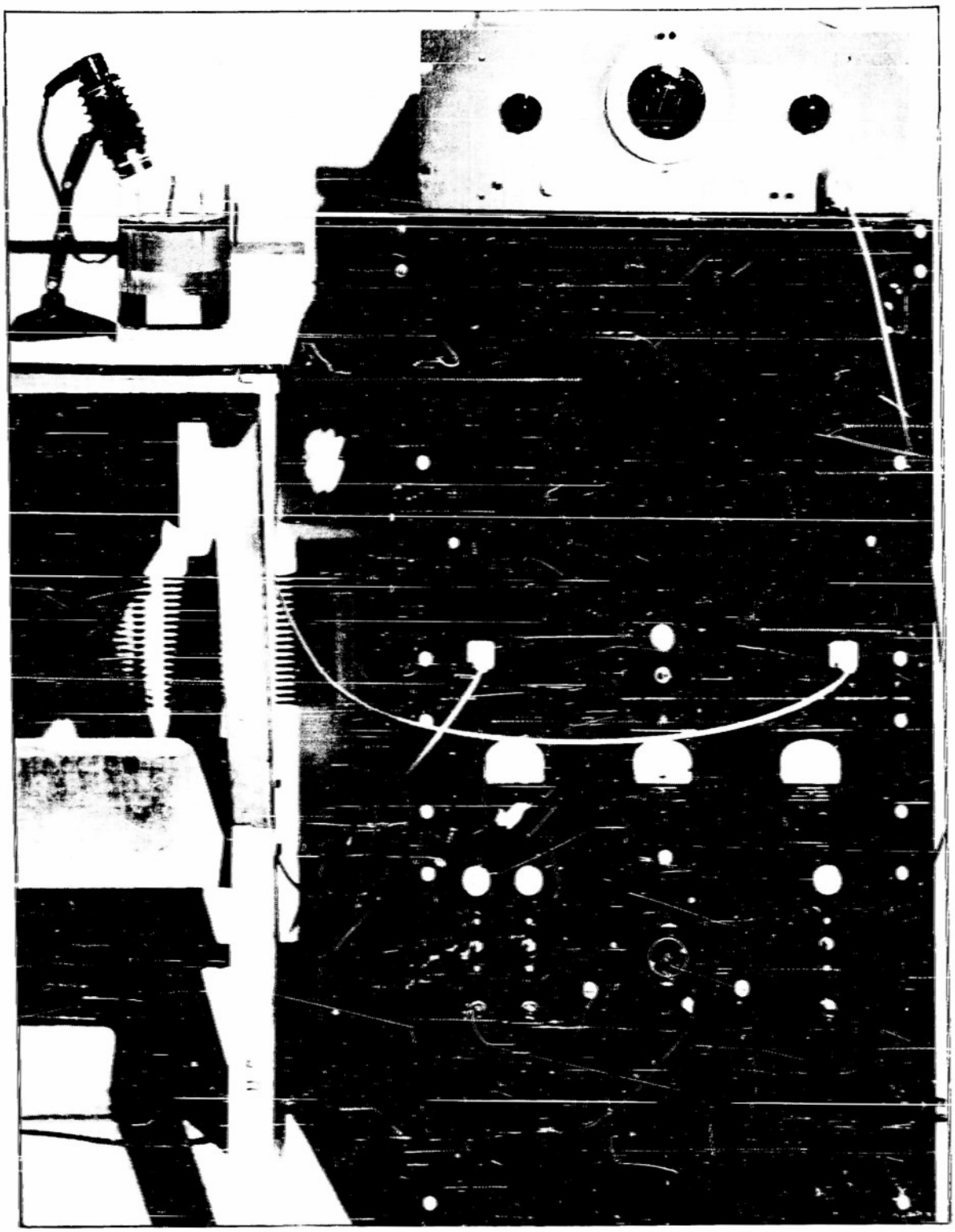

Fig. 3 - Complete apparatus including oscillator, amplifier and beaker.

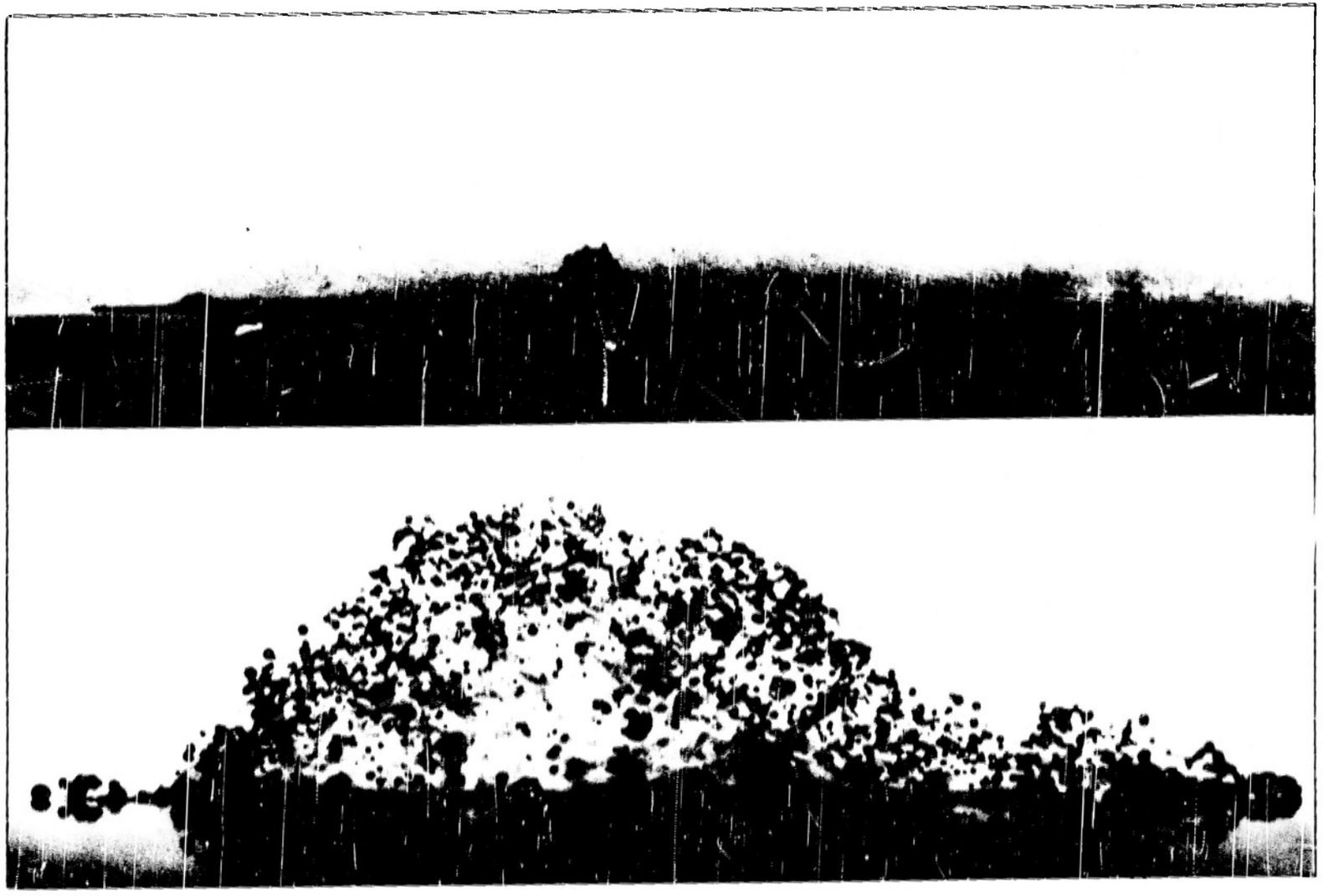

Fig. 4 - The bubble cloud at two different points of the pressure cycle.

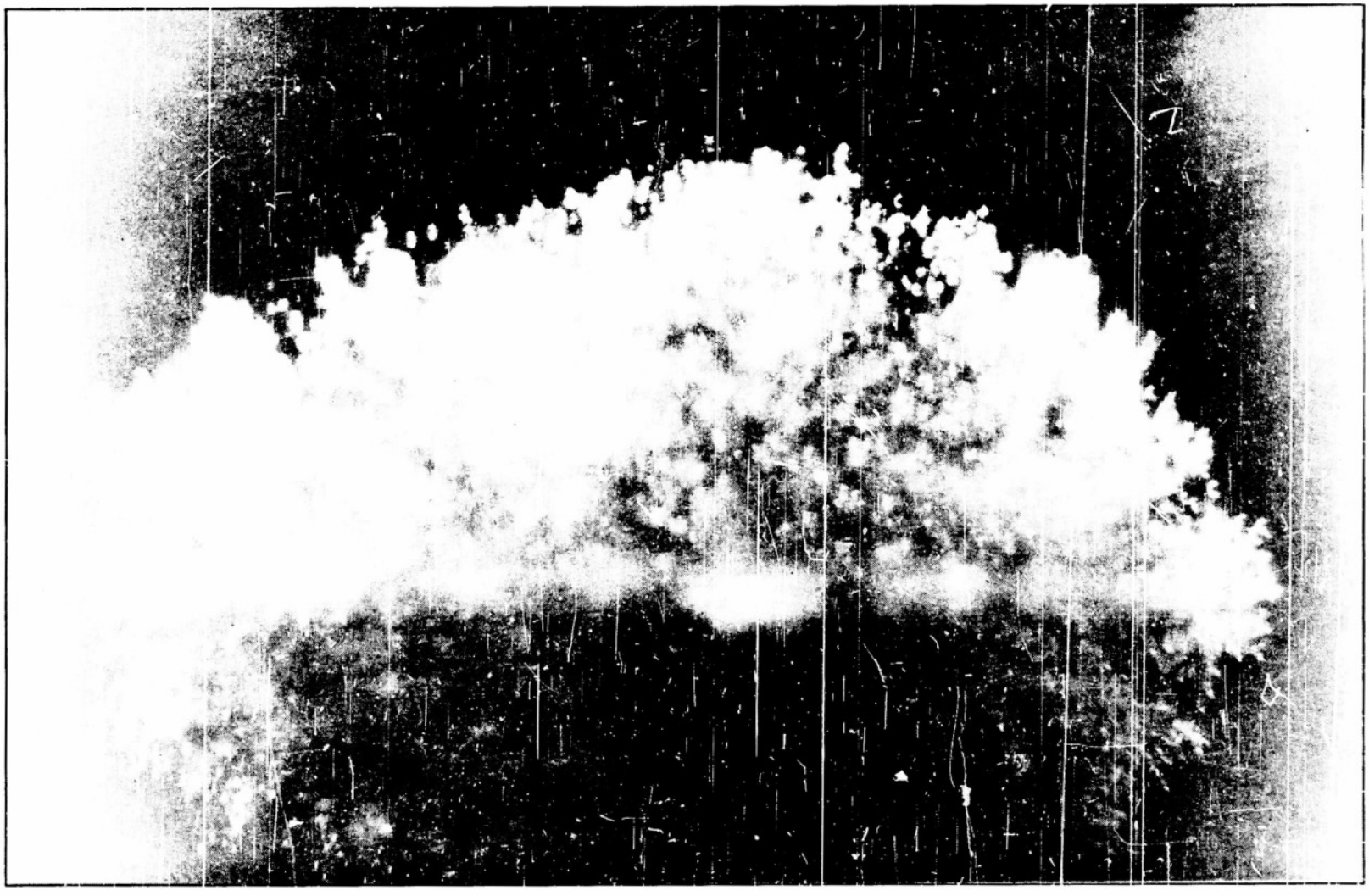

Fig. 5 - Bubble cloud with top lighting.

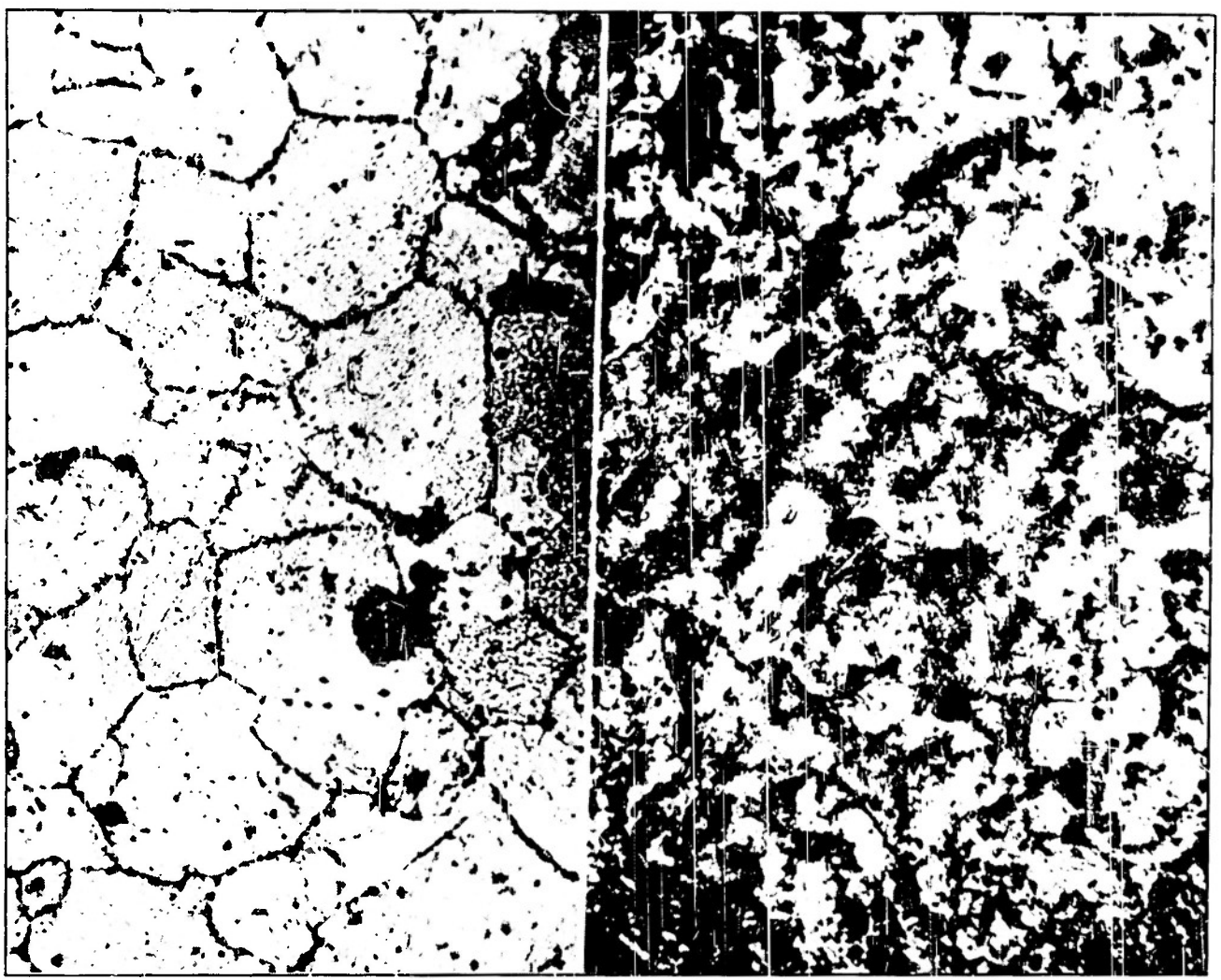

Before exposure to cavitation. After 5 min. exposure to cavitation.

Fig. 6 - Photomicrograph of nickel specimen. Magnification 560X.

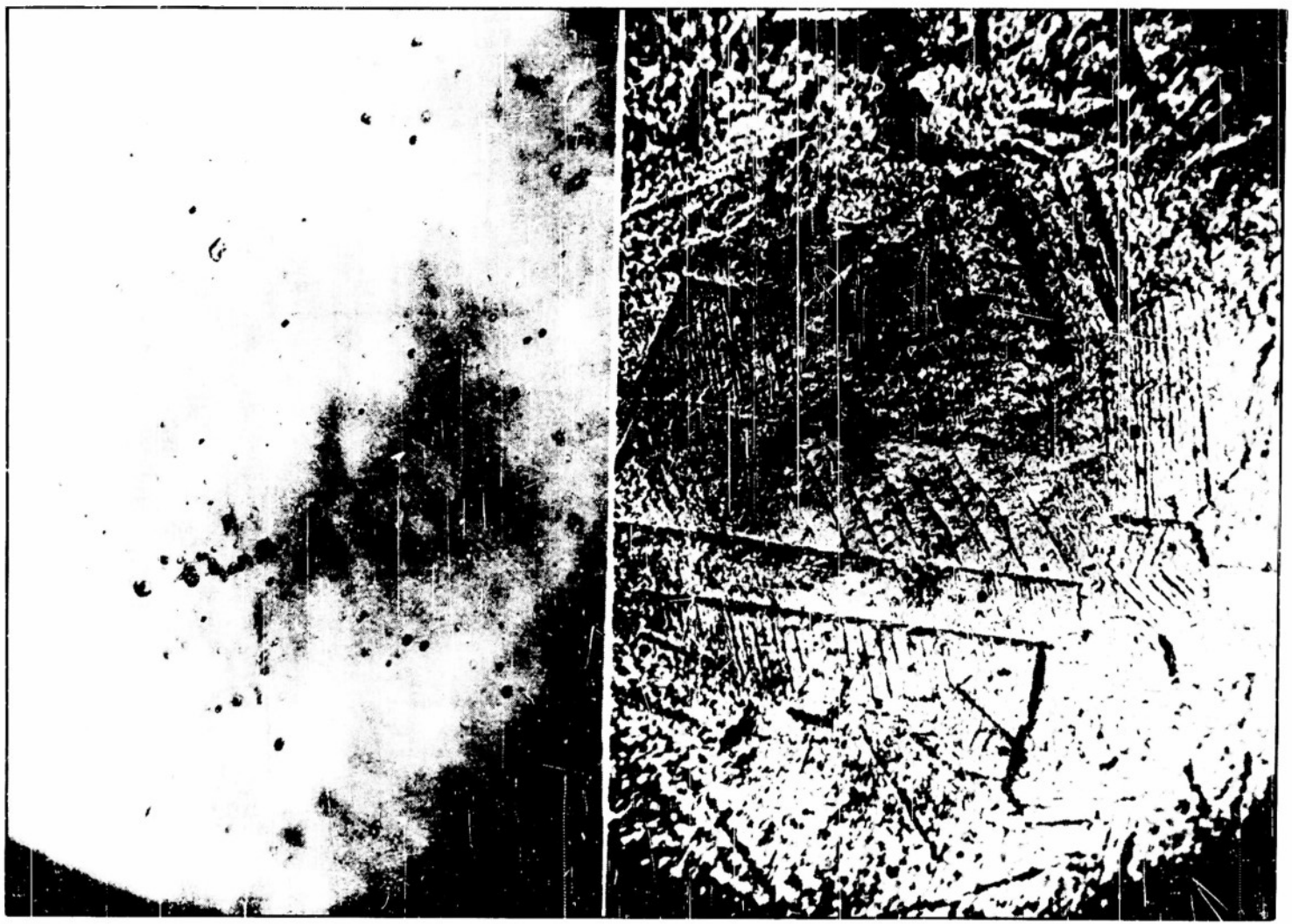

Before exposure to cavitation. After 5 min. exposure to cavitation.

Fig. 7 - Photomicrograph of stainless steel specimen. Magnification 560X.

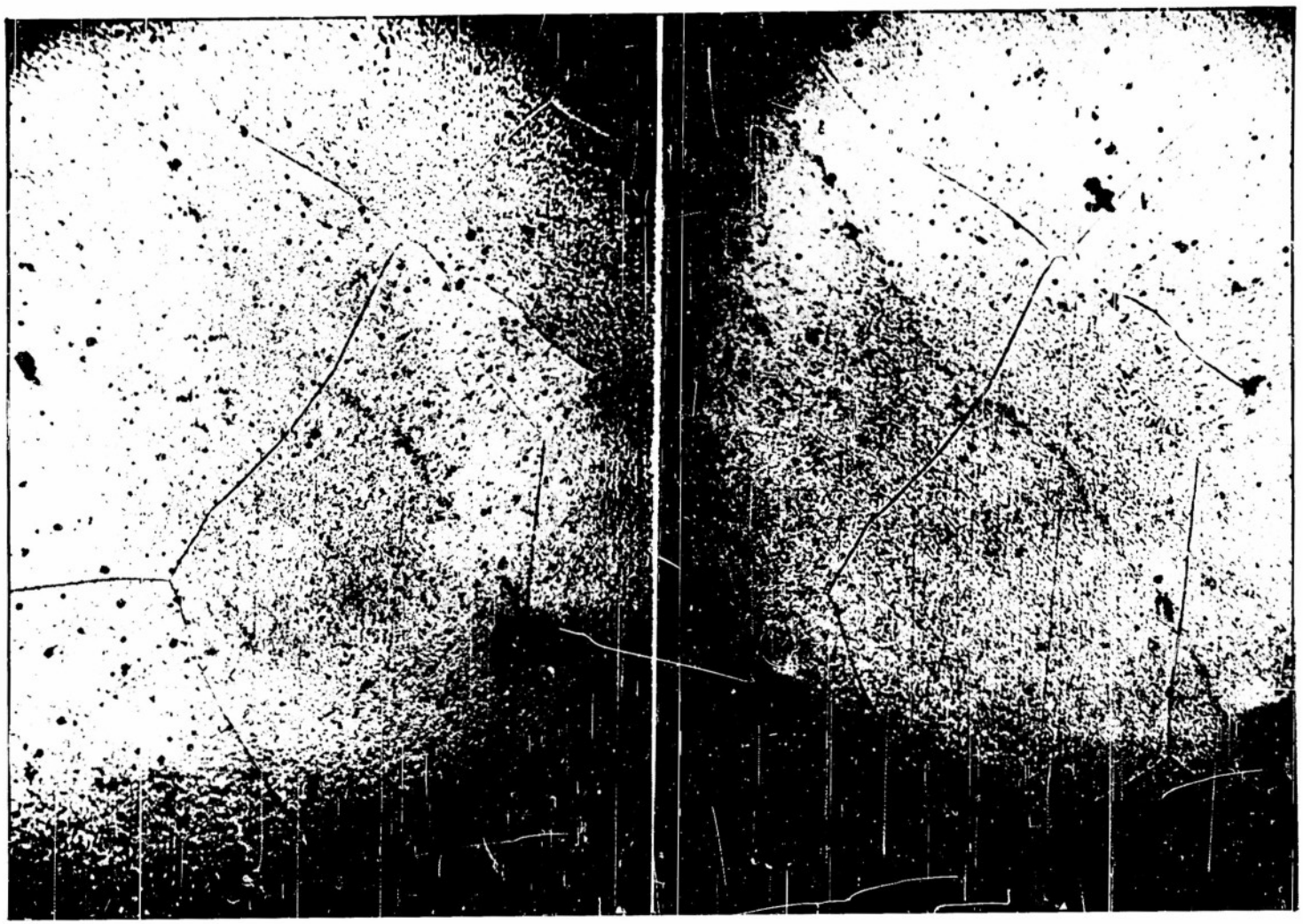

Before exposure to cavitation.

After 2 hr. exposure to cavitation.

Fig. 8 - Photomicrograph of titanium specimen (with 7% manganese). Magnification 200X.

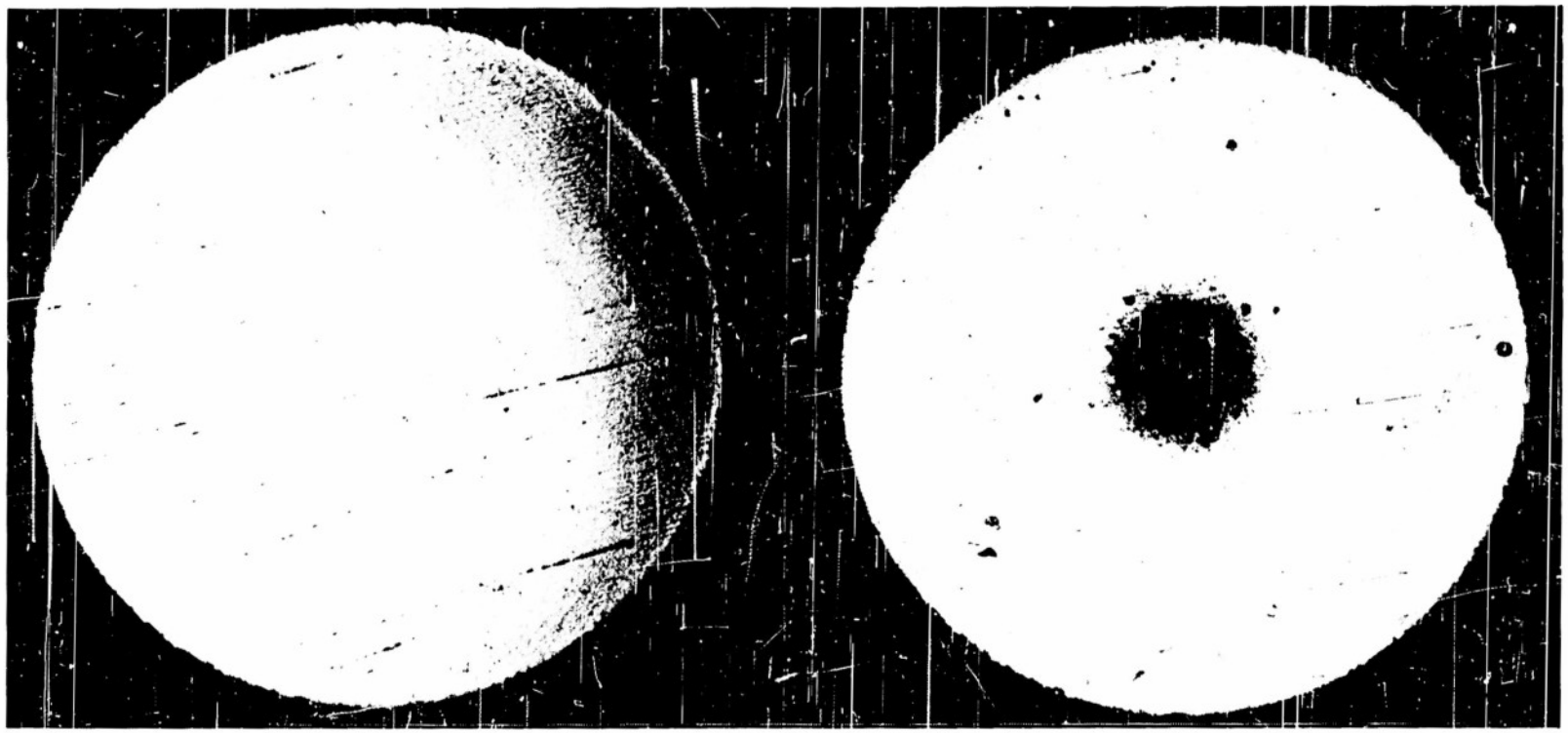

Stellite.
Undamaged.
Magnification 40X.

Stellite.
Damaged 1 hour.
Magnification 40X.

Fig. 9

Titanium 150-A.
Undamaged.
Magnification 40X.

Titanium 150-A.
Damaged 1 hour.
Magnification 40X.

Fig. 10

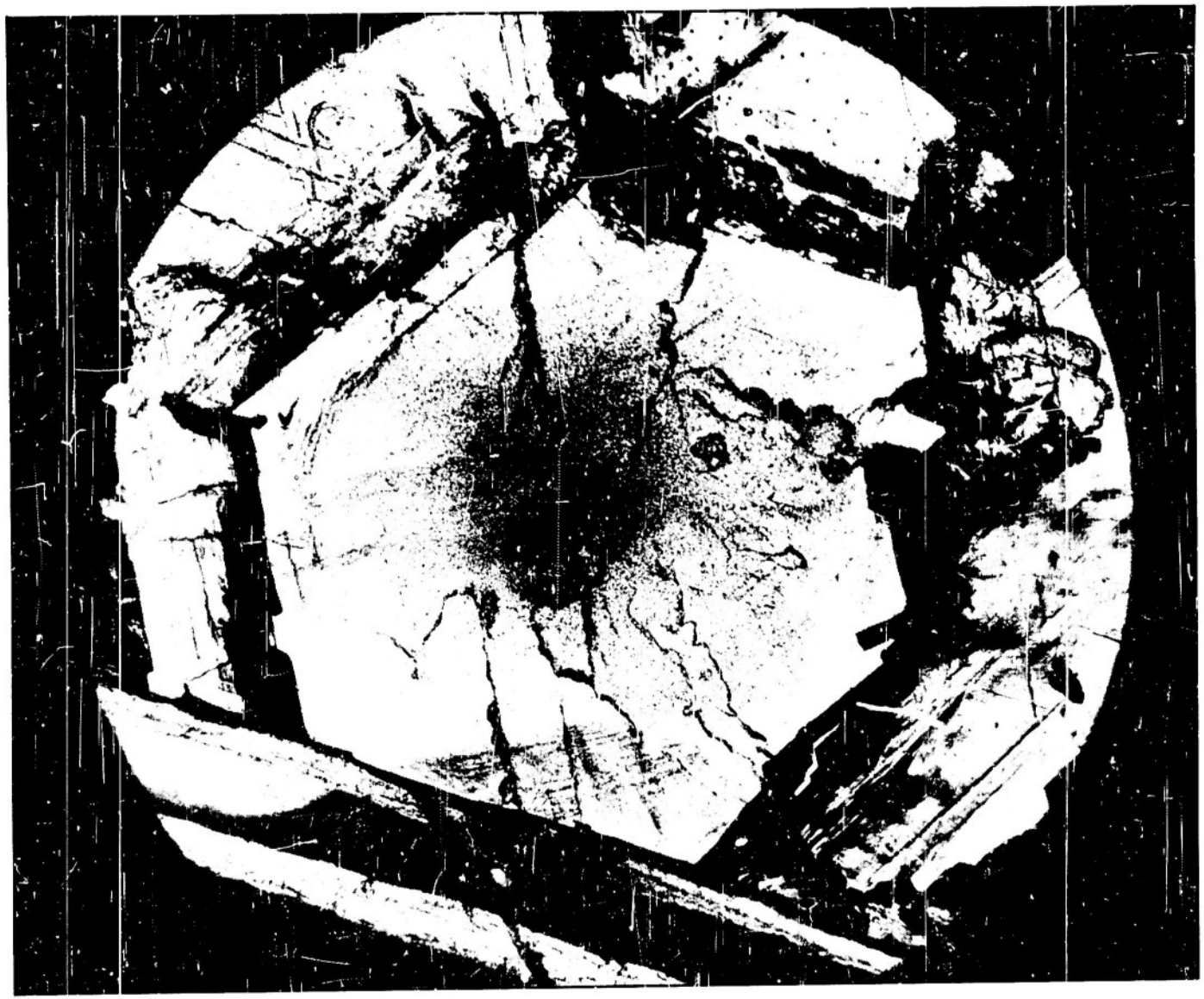

Fig. 11 - Center of damaged area on (0001) plane of a single zinc crystal after 10 min. exposure to 1/16 in. diameter cavitation bubble cloud. Magnification 38X.

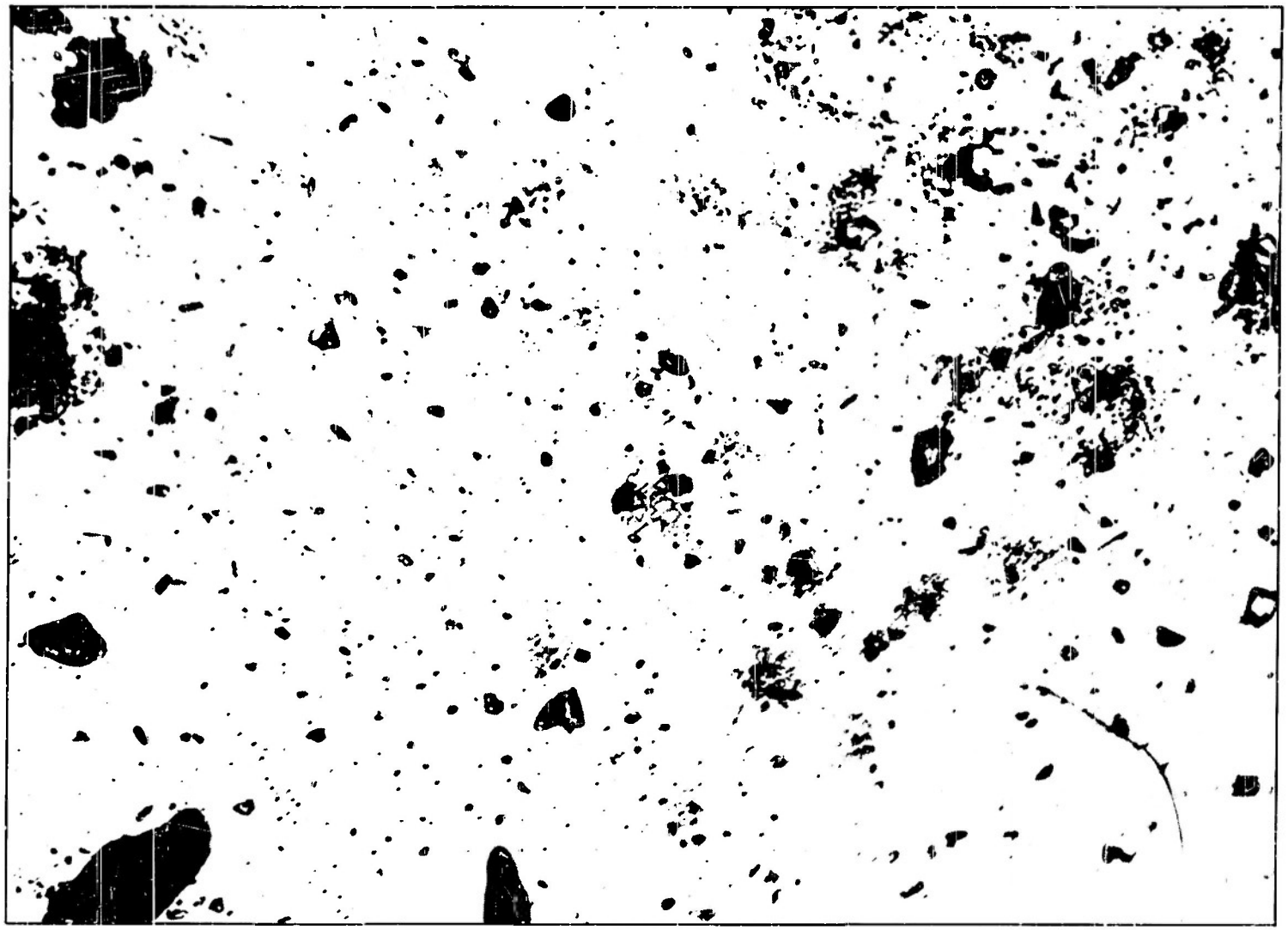

Annealed surface of a zinc monocrystal cleaved along a basal plane.

Fig. 12 - Undamaged. 250X.

Annealed surface of a zinc monocrystal cleaved along a basal plane.

Fig. 13 - Note appearance of many new twin bands, cross twins, and hexagonal pits. 250X, 15 sec. exposure.

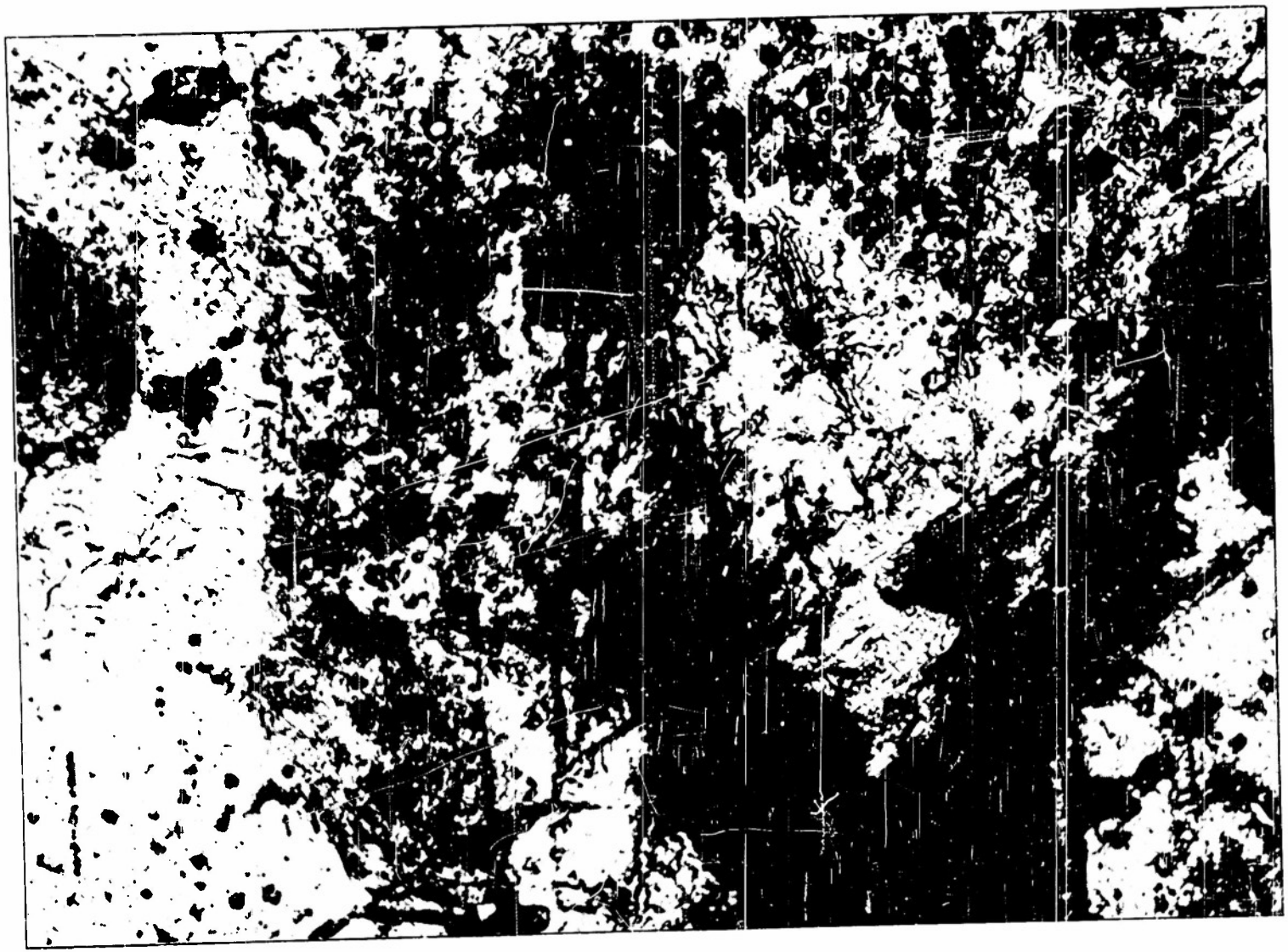

Annealed surface of a zinc monocrystal cleaved along a basal plane.

Fig. 14 - Observe the increase in surface roughness and pitting. 250X, 30 sec. exposure.

Annealed surface of a zinc monocrystal cleaved along a basal plane.

Fig. 15 - Developm. nt of cavitation damage. Note slip lines in twin bands and growth of pits. 100X, 80 sec. exposure.

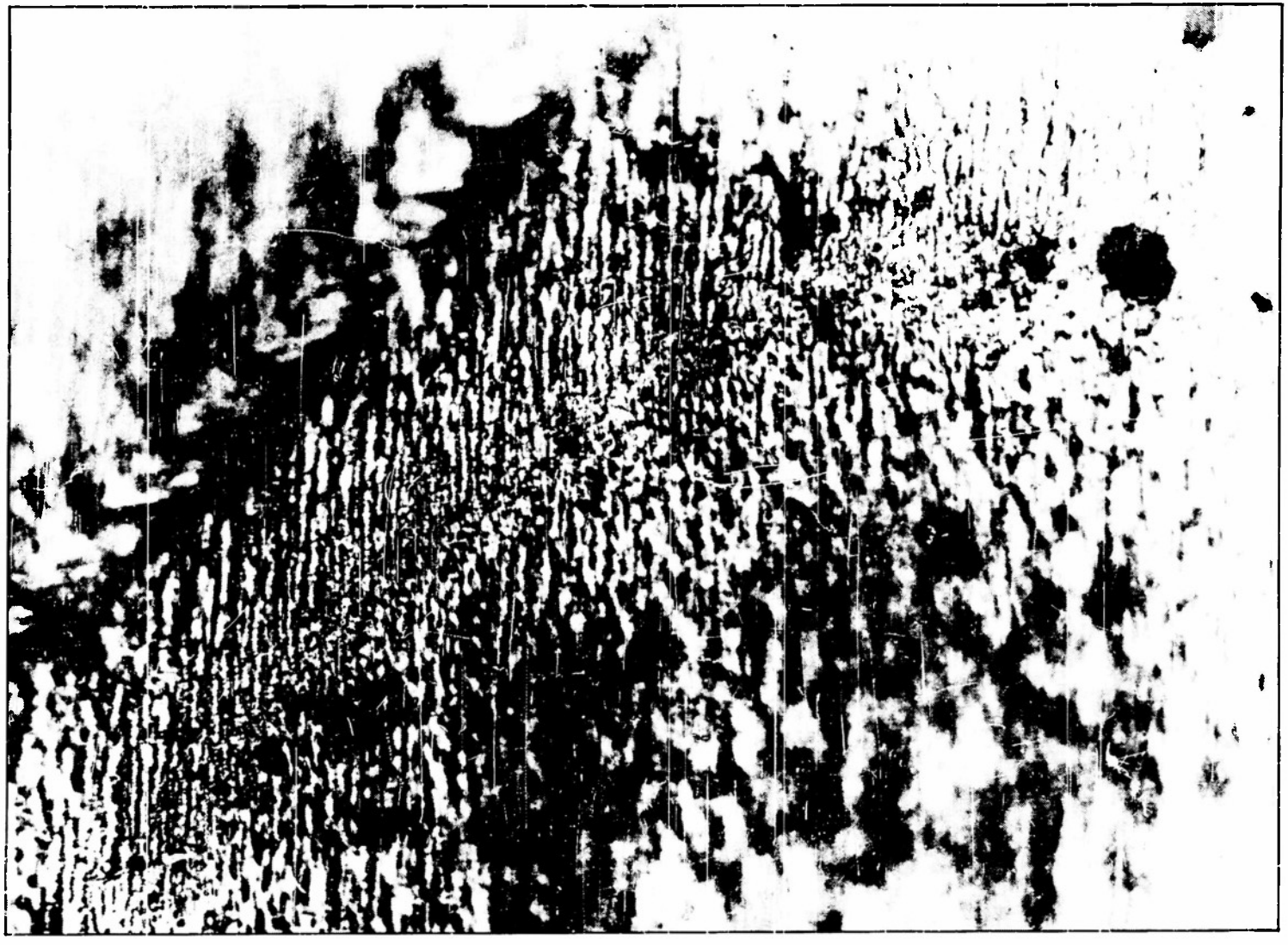

Polished and annealed surface of a zinc monocrystal cut parallel to a twinning plane. Texture of surface is due to preferred attack of etchant. The ropy line across the surface is a twin band due to cutting the specimen.

Fig. 16 - Undamaged. 500X.

Polished and annealed surface of a zinc monocrystal cut parallel to a twinning plane. Texture of surface is due to preferred attack of etchant. The ropy line across the surface is a twin band due to cutting the specimen.

Fig. 17 - Note the rectangular pits in the surface. 500X, 10 sec. exposure.

Polished and annealed surface of a zinc monocrystal cut parallel to a twinning plane. Texture of surface is due to preferred attack of etchant. The ropy line across the surface is a twin band due to cutting the specimen.

Fig. 18 - 500x, 210 sec. exposure.

Geometry of a Zinc Crystal

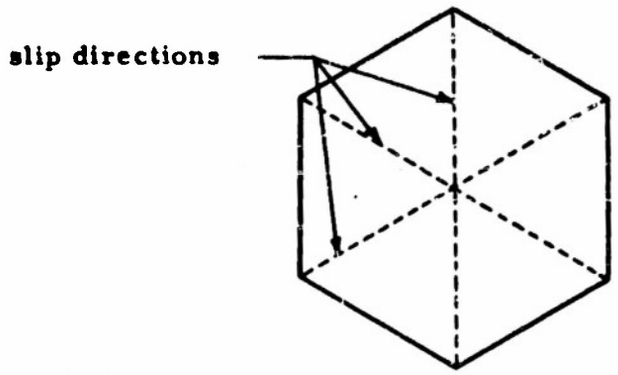

Basal plane projection

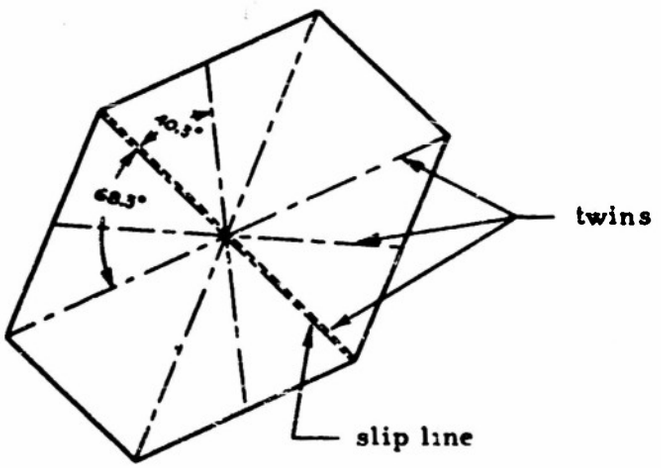

Projection of the twinning plane

twinning plane = $(10\bar{1}2)$
slip plane = (0001)
slip direction = $(11\bar{2}0)$

Fig. 19

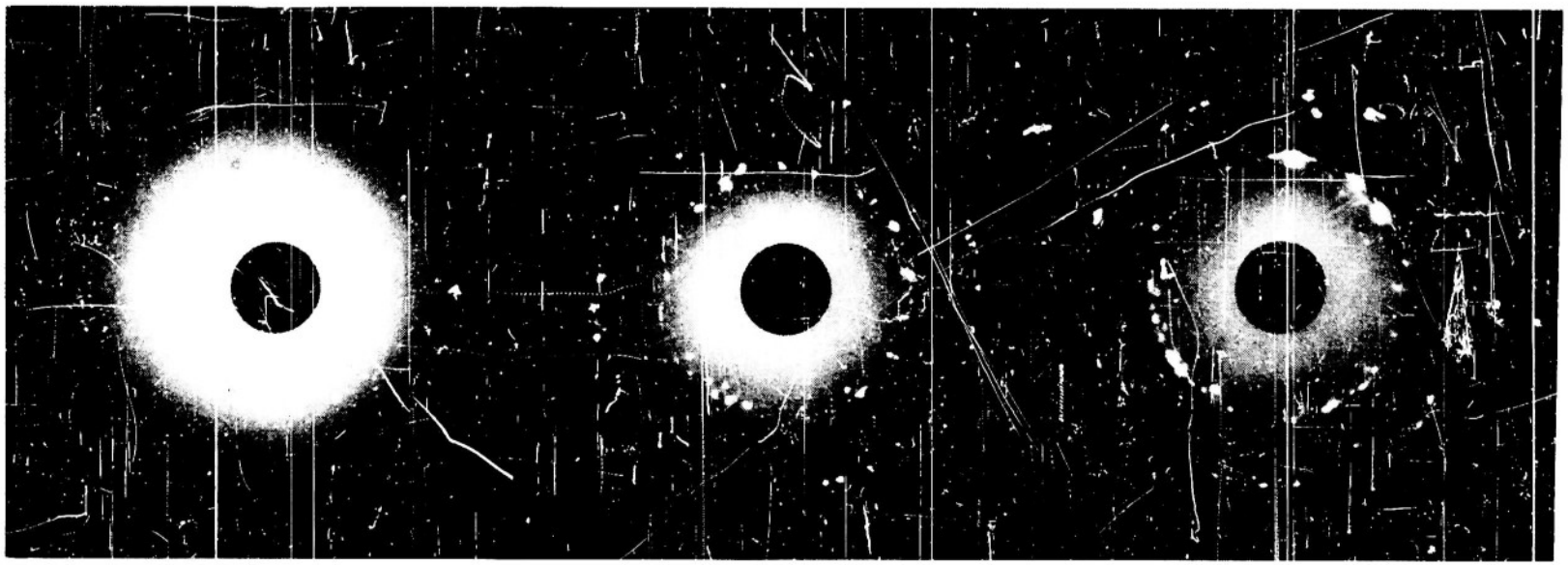

Before exposure to cavitation | After 2 seconds exposure. | After 10 seconds exposure.

Fig. 20 - X-ray diffraction pattern of nickel specimen showing rapid onset of cold work on exposure to cavitation.

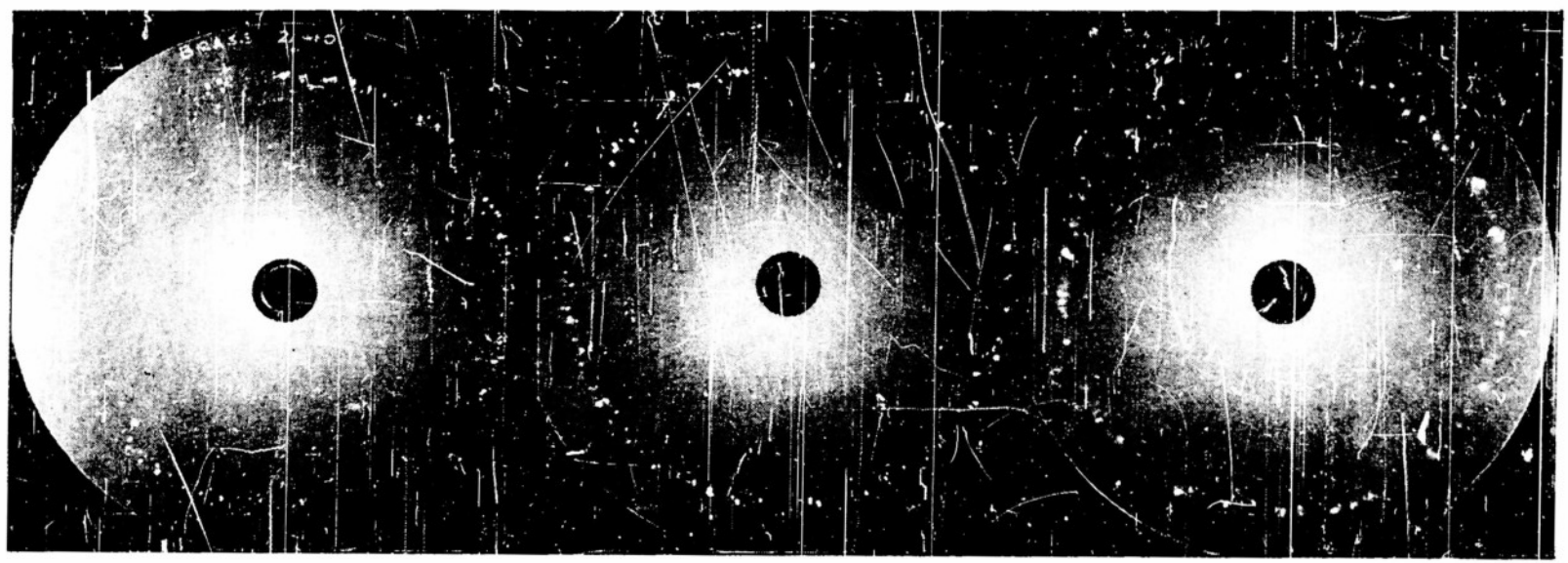

Before exposure to cavitation | After 2 seconds exposure. | After 10 seconds exposure.

Fig. 21 - X-ray diffraction pattern of brass specimen showing rapid onset of cold work on exposure to cavitation.

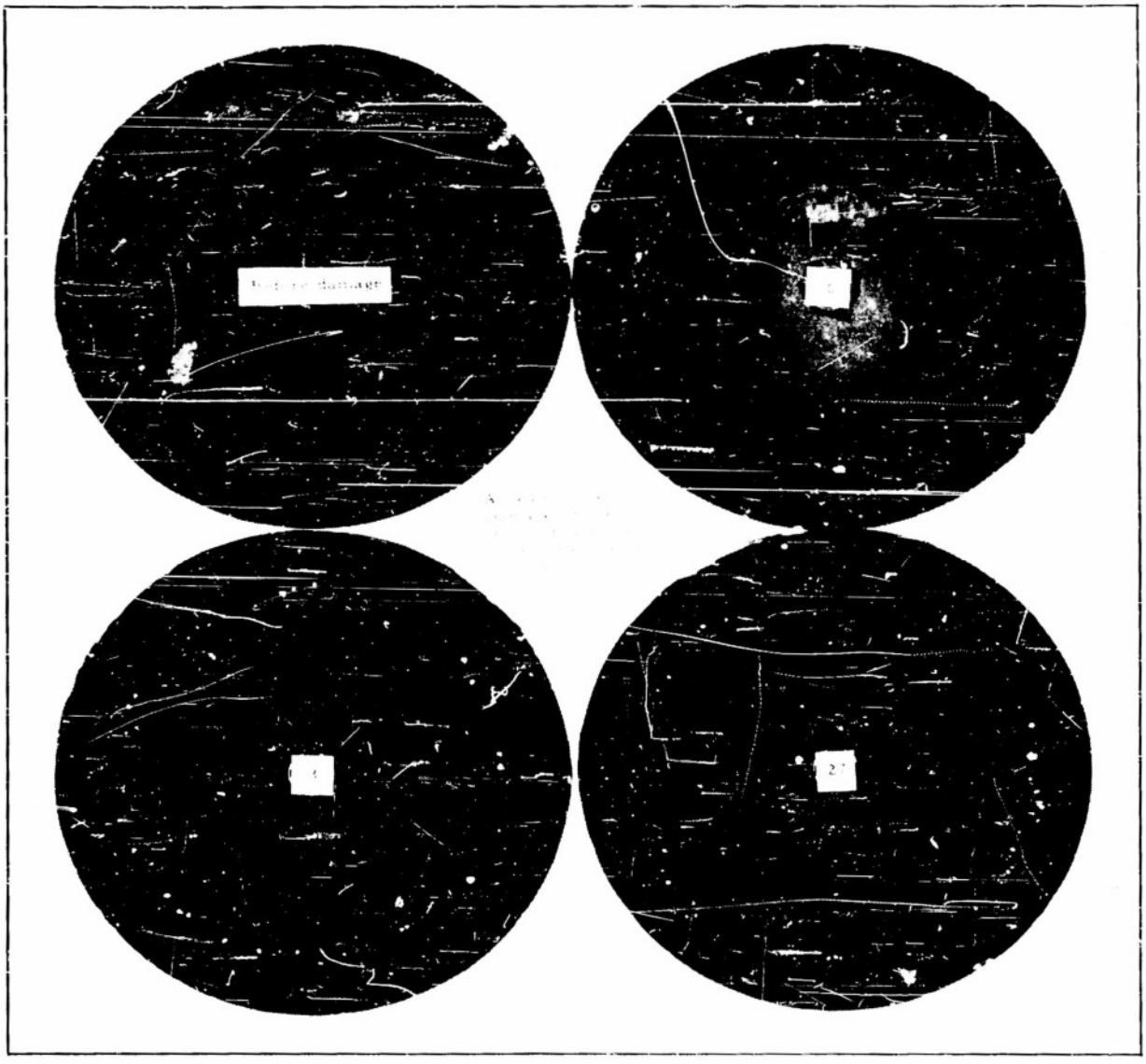

Fig. 22 - Annealed nickel. Damaged 30 secs. Depth of layer removed after damage is shown in microns.

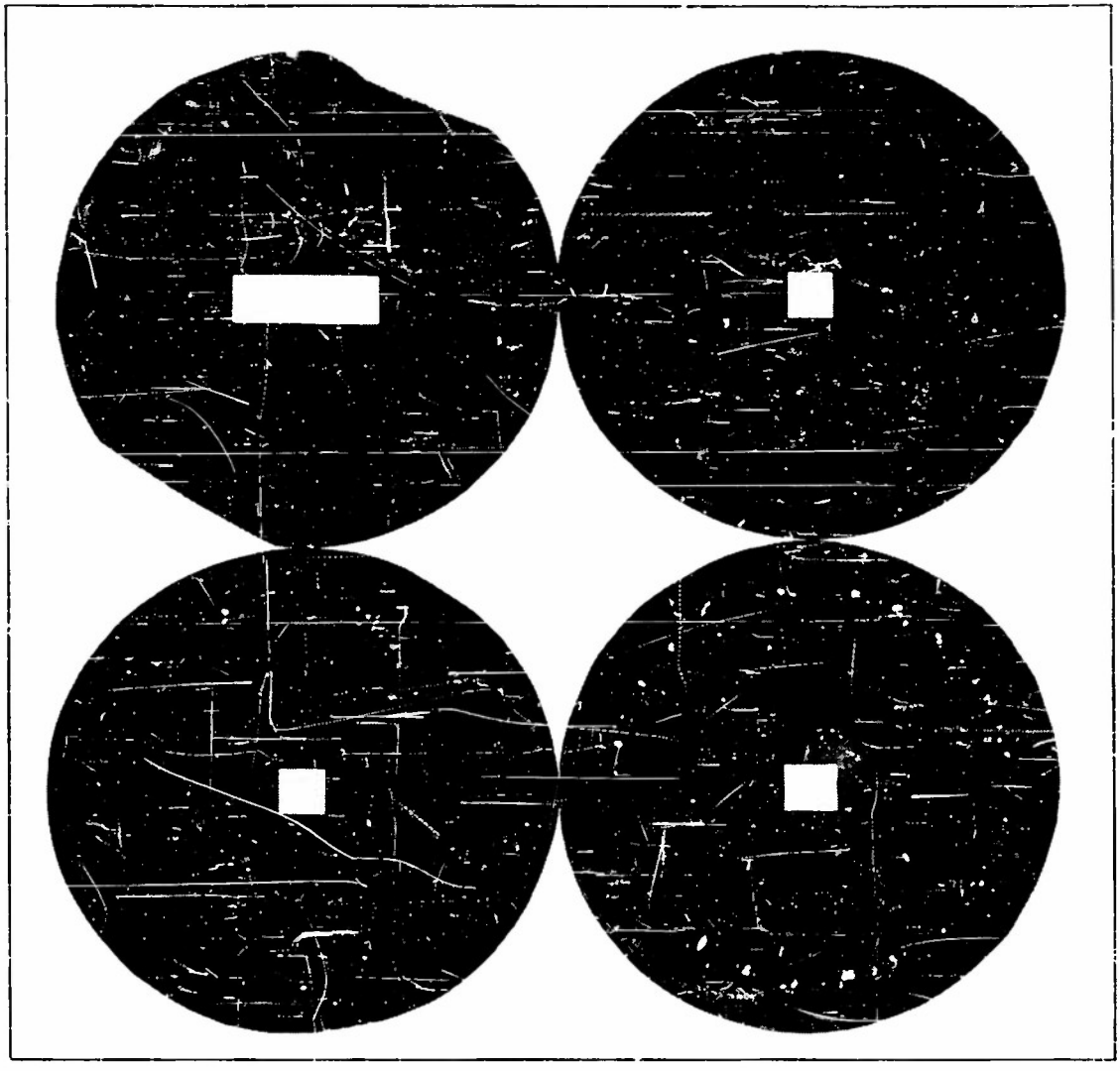

Fig. 23 - Annealed nickel. Damaged 30 min. Depth of layer removed after damage is shown in microns.

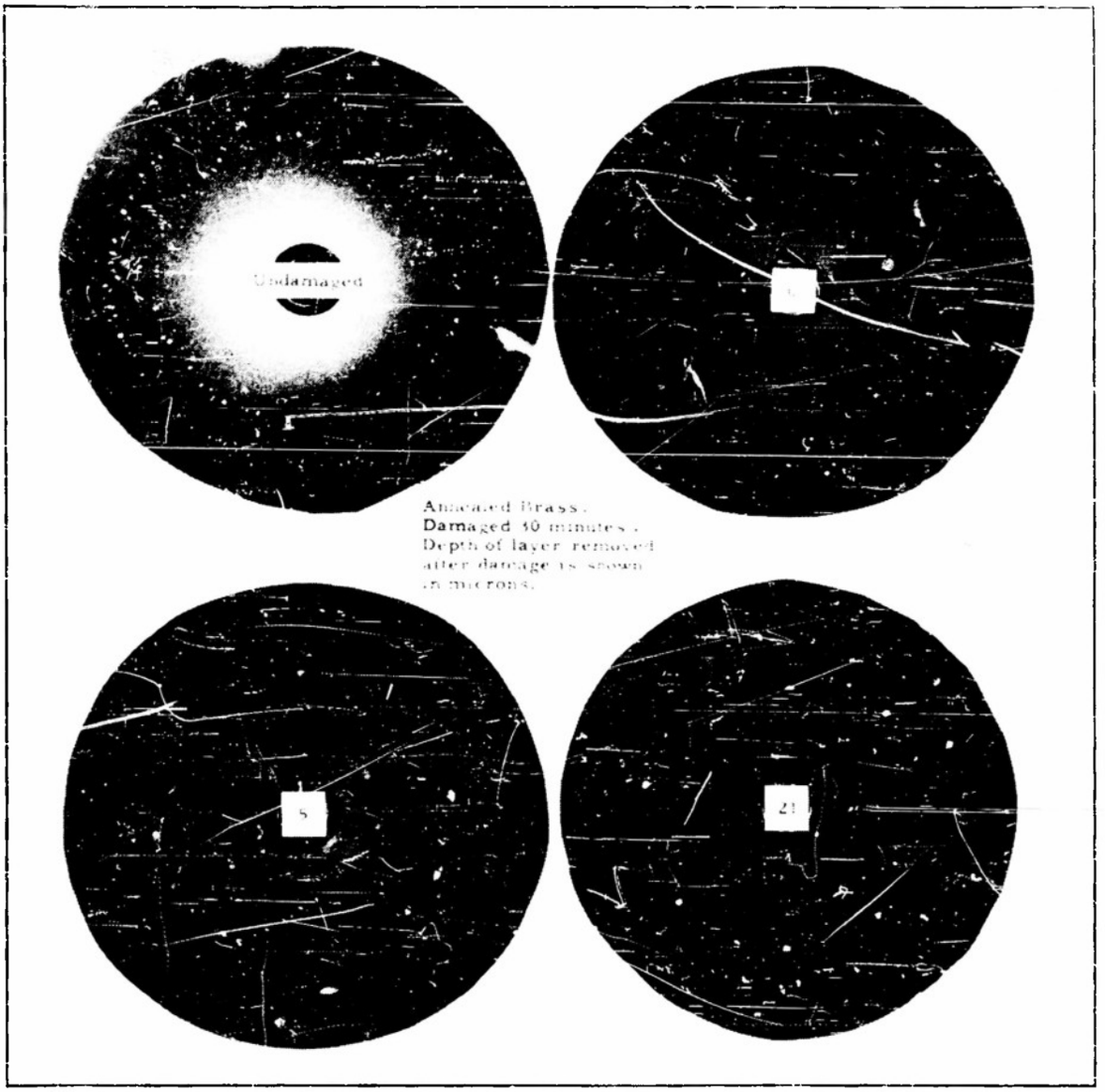

Fig. 24 - Annealed brass. Damaged 30 min. Depth of layer removed after damage is shown in microns.

Fig. 25 - Pure annealed titanium. Damaged 30 min. Depth of layer removed after damage is shown in microns.

TABLE I

Material (arranged in order of increasing hardness)	Composition percent	Hardness (Brinell)	Ultimate tensile strength (psi x 10^3)	Modulus of elasticity (psi x 10^6)	Depth of cavitation damage hole in microns (10^{-4} cm)						
					10 sec	1 min	15 min	30 min	1 hr	2 hrs	3 hrs
Aluminum (soft)		16	16	10	10	80					
Titanium (annealed)		58	79	16			43	78			
Nickel		90	50	30			80	115			
Brass	Cu 70, Zn 30	123	56	13		1	95	128			
Stainless Steel	Cr 18, Ni 8	163	102	29			15	28			
Titanium 75-A		203	80	16					30	66	
Steel (4130)		258	130	30					32	55	
Tungsten		350	597	51				0	0	3	12
Titanium 130-A	Ti 92, Mn 7.9	351	130	16				0	3	16	
Titanium 150-A	Ti 96, Cr 2.7, Fe 1.3	437	150	16				0	0	3	26
Stellite	Co 55, Cr 33, W 6	495	100	36				0	3	14	